

FEDSM-ICNMM2010-' 0+' -

Numerical Investigation of the Flow Field around a Low Rise Building Using LES Technique

S.S. Motallebi Hasankola
School of Mechanical Engineering
Shiraz University, Shiraz, Iran

O. Abouali
School of Mechanical Engineering
Shiraz University, Shiraz, Iran
abouali@shirazu.ac.ir

ABSTRACT

In this research the flow field obtained by LES technique is compared with laboratory data measured around a low rise building model with 1:1:0.3 (length: width: height) aspect ratio. The results also are compared with some other turbulence models. The turbulence models include standard $k-\epsilon$, Durbin's revised $k-\epsilon$ (DBN), and LRR Reynolds stress models (RSM).

Firstly the limitations of the mentioned turbulence models are described for capturing the recirculation zone above and behind of the building model. Among the RANS models, Durbin's revised model with low Reynolds type of the boundary condition predicts the flow field around the building better compared with other RANS models.

The Smagorinski and WALE models among SGS models of LES were employed for the simulation of flowfield around the building. The LES results show generally a better agreement with experimental data compared with RANS models for the streamwise velocity at the roof and behind of building. This improvement is mainly due to the fact that the periodic velocity fluctuation behind the building is well reproduced in LES.

Keyword: turbulence model, LES, low rise building.

INTRODUCTION

In recent years, so many researchers investigated the flow field around the building with different aspect ratios. Also they analyzed some of the turbulence models for the simulation of flow field around the various types of building.

Rodi [1] compared the predicted flow around the square cylinder and three dimensional surface mounted cube with various turbulence modeling such as LES (dynamic and static models) and RANS models. This paper indicates that the

results from the dynamic model of LES show much better agreement with the experimental data than from the others LES and RANS models.

Also he compared reattachment length on behind of the building that a Smagorinsky model of LES predicts the best result (in opposition to the front of building). Also standard $k-\epsilon$ model with wall function boundary condition predicted the reattachment length behind of the cube better than other RANS models. Tominaga et al [2] simulated flow field around a high rise building with various revised $k-\epsilon$ models and LES. They showed among RANS models, DBN model presented most accurate result for the reattachment length at the building top. Also for the reattachment length at behind of building the results of standard $k-\epsilon$ model shows better agreement with experimental data.

Mochida et al [3] investigated the flow field around a high rise building with various forms of $k-\epsilon$ model for both steady and unsteady assumption. Also they presented their results for various schemes of convection terms. Tominaga et al [4] remarked some guidelines for better experimental and numerical simulations around sharp edge bluff bodies such as building. Iaccarino et al. [5] conducted numerical simulation related to the flow field around the surface mounted cube. They used steady and unsteady forms of $k-\epsilon-v^2 f$ model and also LES technique. Results of this study showed that the unsteady form of $k-\epsilon$ model can simulate the flow field with a better accuracy compared with steady form.

The majority of structures built all over the world can be categorized as low-rise buildings used for residential, commercial and other purposes. For this reason, in the present study the flow field around a surface mounted low rise building is simulated numerically and compared with

experimental data [6] that measured in the wind tunnel of Shiraz University.

NOMENCLATURE

$C_{1\varepsilon}, C_{2\varepsilon}, C_\omega$	constant numbers
D	distance to the closest wall
dx, dy, dz	grid dimension of x, y, z direction
K	turbulence kinetic energy
\bar{p}	space- filtered value of static pressure
S_{ij}	strain rate of tensor
SGS	Sub-grid Scale
T	turbulence time scale
U_i	mean velocity components in the x_i direction (i=1; streamwise(x), i=2; lateral(y), i= 3; vertical(z))
U_{ref}	reference value of velocity
\bar{u}_i, \bar{u}_j	space- filtered value of velocity component
u'_i	fluctuation of velocity
X, Y, Z	directions of rectangular coordinate system
X_t, X_r	Reattachment length at the top and behind of the building respectively
x_i	three components of spatial coordinate (i=1;streamwise(x), i=2; lateral(y), i= 3; vertical(z))
τ_{ij}	stress tensor
ν_t	turbulence viscosity
ε	turbulence dissipation rate
μ	viscosity
ρ	fluid density
$(\tau_{ij})_{SGS}$	sub grid stresses tensor
Δt	time step
δ_{ij}	Kronecker delta
K	von-Karman constant
Δ	volume of the computational cell

FLOW FIELD ANALYZED IN THIS STUDY

The flow field around a low-rise building model with 1:1:0.3 (length: width: height) shape and thick inflow boundary layer is selected. Fig .1 shows a schematic of the surface mounted building, wind direction and the coordinate system. The Reynolds number based on h (building height) and U_{ref} (velocity at free stream) was 1.7×10^4 . For this flow field, detailed measurements have been reported by Motallebi et al. [6] using a split-fiber and bi-directional probe. This is a rare database, which consists of the mean and fluctuation velocity around a low rise building with precise inflow boundary condition.

COMPUTATIONAL DOMAIN AND BOUNDARY CONDITION

Flow field around the building is simulated numerically using various turbulence models. According to symmetric condition at the tunnel and body, only half of the domain is considered in the computational domain for the simulation with RANS models.

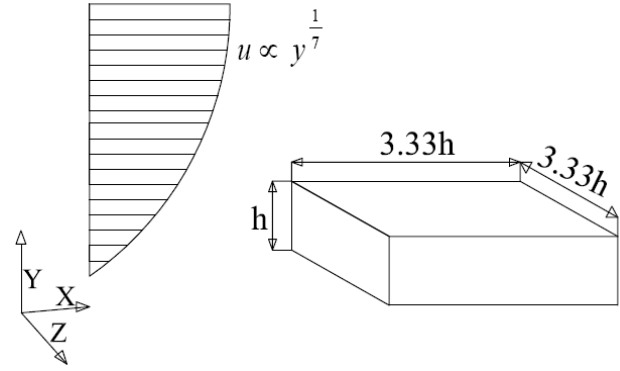


Fig.1: Flow field analyzed for this study.

Fig.2 shows the computational domain and the coordinate system for surface mounted building. According to experimental data the velocity inlet boundary condition was imposed on surface IMQL which the mean velocity and the distribution of turbulence intensity are shown in Fig.3. The wall boundary condition was used for surfaces of MQPN, MNJI, LQPK and building walls. Since the distance between body and JNPK surface is large enough, the outflow can be considered fully developed.

Grid generation approach was used with a very dense grid near to the building and a coarse grid far from it. The numbers of the grid for the wall function boundary condition is 230000, but for low Reynolds boundary condition the grid size is 2300000. These grid sizes resulted by the grid study.

But for simulation with the LES technique whole of the domain is considered as this technique is unsteady and do not exist symmetry condition especially behind the building (existence of vortex shedding).

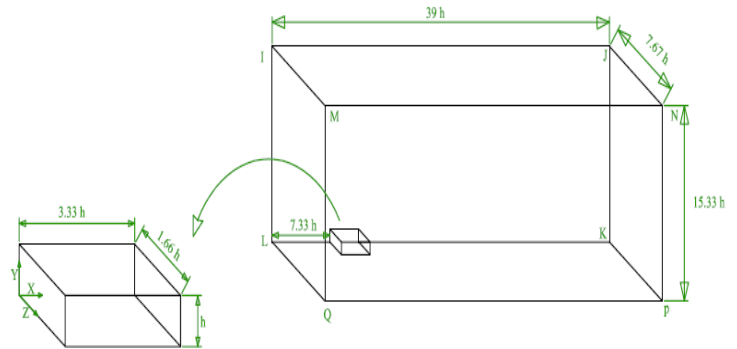


Fig.2: Computational domain and location of building and coordinate system.

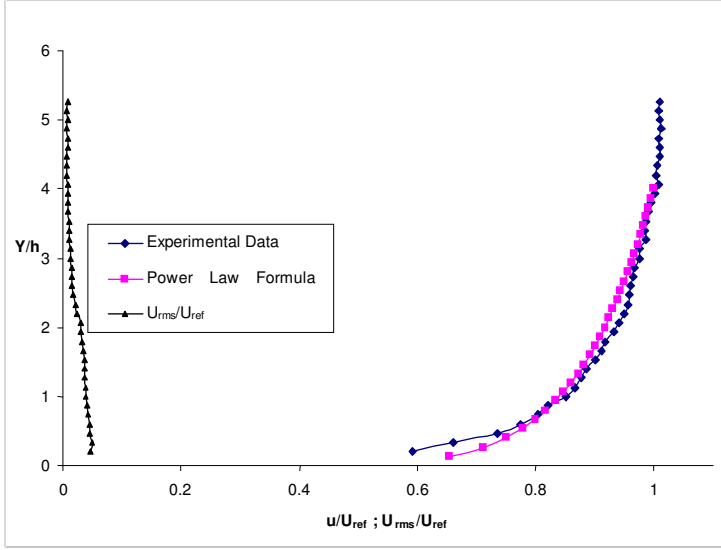


Fig.3: Velocity and turbulence intensity for inflow boundary condition.

GOVERNING EQUATION

Reynolds averaged Navier-Stokes for steady and incompressible flow can be expressed as:

$$\frac{\partial U_i}{\partial x_i} = 0 \quad (1)$$

$$U_j \frac{\partial U_i}{\partial x_j} = -\frac{1}{\rho} \frac{\partial P}{\partial x_i} - \frac{\partial \overline{u_i' u_j'}}{\partial x_j} + \nu \frac{\partial^2 U_i}{\partial x_j^2} \quad (2)$$

$$\tau_{ij}^T = -\rho \overline{u_i' u_j'} \quad (3)$$

$$\tau_{ij} = 2\nu_t S_{ij} - \frac{2}{3} k \delta_{ij} \quad (4)$$

At this equation τ_{ij} is Reynolds stress tensor that computed by Boussinesq approximation. Kato and Launder presented their well known standard $k-\epsilon$ model by following formula [7]:

$$\frac{\partial}{\partial t}(\rho k) + \frac{\partial}{\partial x_i}(\rho k u_i) = \frac{\partial}{\partial x_j} \left[\left(\mu + \frac{\mu_t}{\sigma_k} \right) \frac{\partial k}{\partial x_j} \right] + \mu_t S^2 - \rho \epsilon \quad (5)$$

$$\frac{\partial}{\partial t}(\rho \epsilon) + \frac{\partial}{\partial x_i}(\rho \epsilon u_i) = \frac{\partial}{\partial x_j} \left[\left(\mu + \frac{\mu_t}{\sigma_\epsilon} \right) \frac{\partial \epsilon}{\partial x_j} \right] + C_{1\epsilon} \frac{\epsilon}{k} (\mu_t S^2) - C_{2\epsilon} \rho \frac{\epsilon^2}{k} \quad (6)$$

In these equations, S is strain rate tensor.

Many researchers have shown that the application of the standard $k-\epsilon$ model for the flow field around bluff bodies often yields critical error such as overestimation of turbulent kinetic energy in the impinging region [8] and [9]. Numerous models were developed to solve the mentioned problem.

Durbin [10] presented a revised $k-\epsilon$ model in which the time scale of turbulence was constraint by the following expressions:

$$T = \min(T_s, T_D) \quad (7)$$

$$T_s = \left(\frac{k}{\epsilon} \right) \quad (8)$$

$$T_D = \frac{1}{C_\mu S \sqrt{3}} \quad (9)$$

Many problems reported for simulation of complex flows with Boussinesq approximation. In present work also one type Reynolds Stress models (RSM) is used. In these models Boussinesq approximation is not used and for each component of Reynolds stress tensor a differential equation is being used. LRR (Launder - Reece- Rodi) model is used in present work [11].

Both type of the wall boundary condition such as wall function and low Reynolds type are performed in this research.

LES methods resolve large eddies (i.e. the energy-containing eddies) explicitly, whereas only small eddies (i.e. energy-dissipating eddies) are modeled. Also, LES is a time dependent calculation. therefore it provides a significant quantity of flow data for statistical analysis. The governing equations of LES are as follow [11]:

$$\frac{\partial \bar{u}_i}{\partial x_i} = 0 \quad (10)$$

$$\frac{\partial \bar{u}_i}{\partial t} + \frac{\partial (\bar{u}_i \bar{u}_j)}{\partial x_j} = -\frac{1}{\rho} \frac{\partial \bar{P}}{\partial x_i} + \frac{\partial}{\partial x_j} \left[\frac{\mu}{\rho} \left(\frac{\partial \bar{u}_i}{\partial x_j} + \frac{\partial \bar{u}_j}{\partial x_i} \right) \right] - \quad (11)$$

$$\frac{1}{\rho} \frac{\partial (\tau_{ij})_{SGS}}{\partial x_j}$$

Where $(\tau_{ij})_{SGS}$ represents the sub-grid stresses. The sub-grid stresses can be modeled by a number of sub-grid models. One of the widely used sub-grid models is the Smagorinsky model [12], which evaluates the sub-grid stresses by a simple relation as following:

$$(\tau_{ij})_{SGS} = -2\mu_{SGS} \bar{S}_{ij} \quad (12)$$

$$\mu_{SGS} = \rho (C_s \Delta)^2 (\bar{S}_{ij} \bar{S}_{ij})^{1/2} \quad (13)$$

$$\bar{S}_{ij} = \frac{1}{2} \left(\frac{\partial \bar{u}_i}{\partial x_j} + \frac{\partial \bar{u}_j}{\partial x_i} \right) \quad (14)$$

Where C_s is the Smagorinsky constant and Δ is the characteristic length of a computational grid. This study used $C_s = 0.12$ and $\Delta = (dx \times dy \times dz)^{1/3}$ to calculate the sub-grid stresses.

The second-order central differencing scheme was applied in equation (11) for spatial discretization. The temporal differencing schemes used for the convection terms and the diffusion terms were the Adam–Bashforth and the Crank–Nicolson schemes, respectively.

The following equations present the wall-adapting local eddy-viscosity (WALE) model that is another popular SGS model [13]:

$$\mu_t = \rho L_s^2 \left(\frac{(S_{ij}^d S_{ij}^d)^{3/2}}{(\bar{S}_{ij} \bar{S}_{ij})^{5/2} + (S_{ij}^d S_{ij}^d)^{5/4}} \right) \quad (15)$$

Where L_s and S_{ij}^d are defined respectively as following:

$$L_s = \text{Min}(\kappa d, C_\omega \Delta^{1/3}) \quad (16)$$

$$S_{ij}^d = \frac{1}{2} (\bar{g}_{ij}^2 + \bar{g}_{ji}^2) - \frac{1}{3} \delta_{ij} \bar{g}_{kk}^2 \quad (17)$$

$$\bar{g}_{ij} = \frac{\partial \bar{u}_i}{\partial x_j} \quad (18)$$

In the equation (16) C_ω is a constant and equals to 0.325. Also κ is the von-Karman constant, d is the distance to the closest wall. With this spatial operator, the WALE model is designed to return the correct wall asymptotic (y^3) behavior for wall bounded flows.

A small time step was required to ensure numerical stability. Therefore, the value $\Delta t = 0.01 \frac{h}{U_{ref}}$ was used in order to complete the calculations. The time averaged values were determined by time averaging over a 10000 time step (Δt).

RESULT AND DISSCUSION

COMPARISON OF RANS MODELS

Table1 shows the resulted reattachment lengths for various turbulence models in the roof X_t and behind of the building, X_r . Fig.4 shows a schematic of reattachment length in the top and behind of the building. Clearly, no reverse flow is observed on the roof when wall function boundary condition was used as for the standard $k-\epsilon$ model is pointed out in previous researches by the authors' group [8], [9] and [12]. While each model with low Reynolds wall boundary condition reveals such a reverse flow. Except DBN model, the reattachment length obtained by other models is overestimated compared with experimental data.

In contrary to previous results for the roof wall, the reattachment length behind the building, X_r , is larger than the

experimental value in all cases compared here. It should be noted that the RANS models with wall function boundary condition tend to evaluate X_r larger than these models with low Reynolds boundary condition.

Among all studied turbulence models, LRR with wall function boundary condition shows the best agreement with experimentally measured reattachment length behind the building. Also the DBN model with low Reynolds boundary condition presented better prediction compared to LRR and $k-\epsilon$ model with this boundary condition.

Since the flow around the building is complex, just comparison of the reattachment length is not enough. Because of the rough prediction of wall boundary condition especially for the roof of the building, only results of low Reynolds wall boundary condition will be shown for further results.

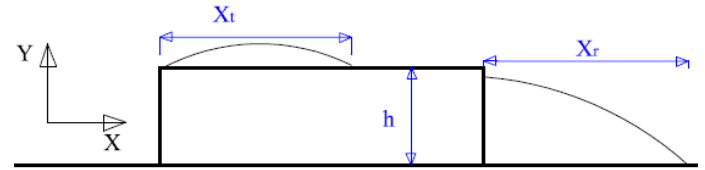


Fig. 4: Reattachment length in the top and behind of the building.

Table1. Comparison of various turbulence models with experimental data.

Type of Model	Type of Boundary Cond.	X_t/h	X_r/h
$k-\epsilon$	Wall Function	0	3
DBN	Wall Function	0	3.33
LRR(RSM)	Wall Function	0	2.5
$k-\epsilon$	Low Reynolds	0.83	3.8
DBN	Low Reynolds	0.41	3.33
LRR (RSM)	Low Reynolds	1.26	3.42
Exp [6].	-----	0.533	2.44

The vertical distributions of the streamwise component of velocity above and behind the building are illustrated in Fig.5-Fig.8.

Fig.5 indicates the velocity profiles on the roof of the surface mounted building at $X/h=0$ which a defect can be observed in the vicinity of $Y/h = 1.2$ in the experimental data. The turbulence models can not predict this defect but out of this region the DBN model simulation is better than that for other models relative to the experimental data.

Fig.6 shows the streamwise velocity on the roof of the building at $X/h=0.33$ which the defect still exist in the experimental data. The DBN model shows closest result to the experimental data.

The same comparison between the stream wise velocity obtained by various models and experimental data at the $X/h=1.66$ is presented in Fig.7. The models predictions depict a similar trend. Here the DBN model presents a better

prediction. LRR and $k-\epsilon$ models predicted a large recirculation zone wrongly in this location.

The streamwise velocity along a vertical line located in the reversed flow in behind of the surface mounted building $X/h=3.66$ is shown in Fig.8. The numerical models roughly could predict the defect of the velocity profile but generally DBN model present a more accurate result.

The same comparison is shown in Fig.9 for the location of $X/h=5.66$. In this location, the height of recirculation zone is bigger than that in experiment The prediction of DBN model is better relative to the other models.

As the result of numerical model for flow around the surface mounted building showed the low Reynolds boundary condition is preferred to wall function because the latter can not reproduce reverse flow on the roof of the building. Also according to reattachment length and flow field, DBN model presented the best accuracy among studied turbulence models.

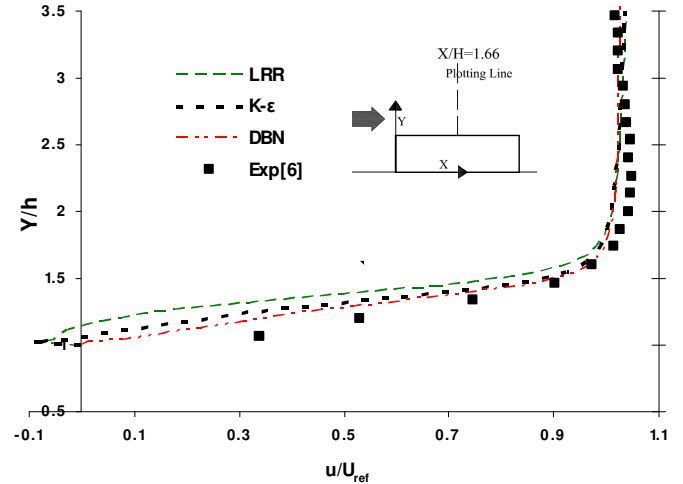


Fig.7: Vertical distribution of streamwise velocity above the building at $X/h=1.66$

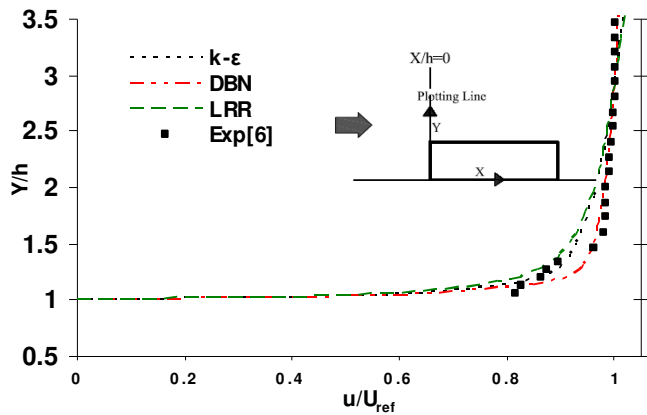


Fig.5: Streamwise velocity distribution above the building at $X/h=0$

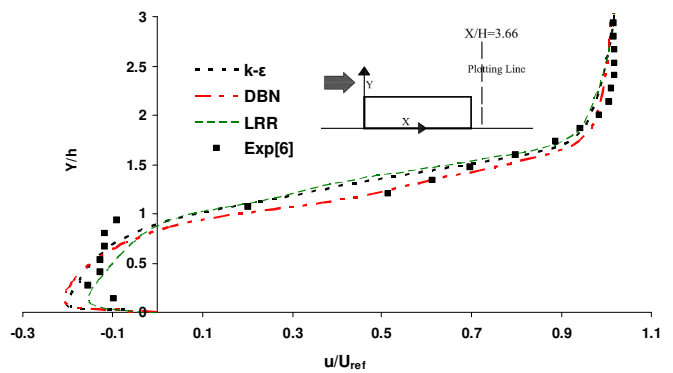


Fig.8: Streamwise velocity distribution above the building at $X/h=3.66$

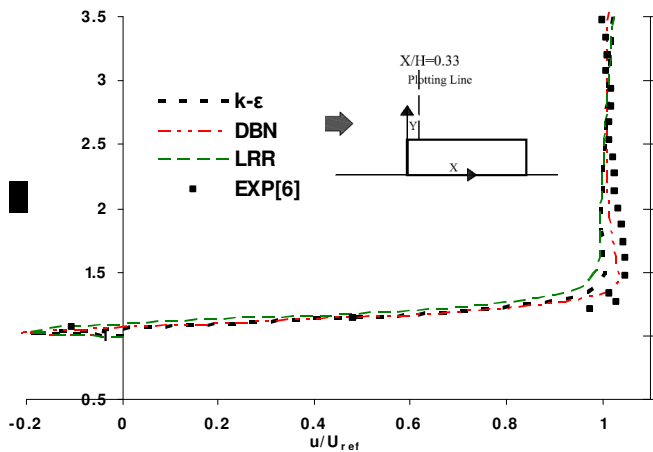


Fig.6: Streamwise velocity distribution above the building at $X/h=0.33$

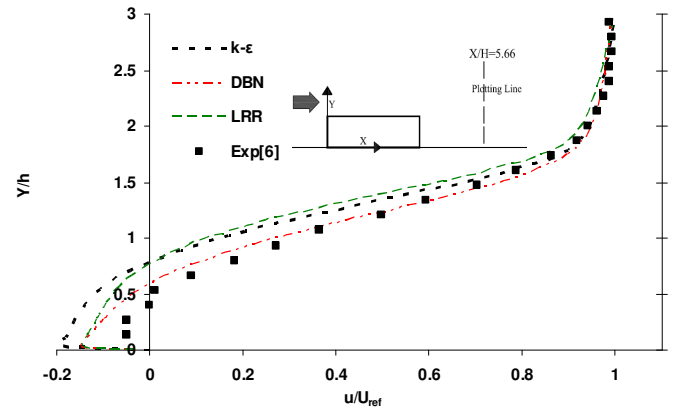


Fig.9: Streamwise velocity distribution above the building at $X/h=5.66$.

COMPARISON BETWEEN DBN MODEL AND LES

Table 2 shows the predicted reattachment lengths, X_r (on the roof) and X_r (behind the building) for the Smagorinsky and WALE models of LES computations. The results of the revised $k-\varepsilon$ model (DBN), which shows the closest agreement with the experimental data among various RANS models compared in the previous section, are also shown. The reverse flow on the roof has captured in the results of two mentioned model of LES technique. The reattachment length on the roof with Smagorinsky model is overestimated. The WALE model underestimated the reattachment length on the roof but presents a better result compared with DBN model.

As already mentioned, the reattachment length behind the building, X_r , is greatly overestimated in DBN model. This discrepancy is improved for the Smagorinsky model of LES computation as it is predicted almost exactly. The WALE model of LES overestimated this length with small difference.

Table2. Comparison of LES results with experimental data.

Type of Model	X_r/h	X_r/h
LES Smagorinsky	0.64	2.43
LES WALE	0.45	2.56
DBN (Low Reynolds)	0.41	3.33
Exp [6].	0.533	2.44

Fig.10–14 show the comparison between DBN model and Smagorinsky and WALE models of LES for streamwise velocity on the roof and behind of building. As already mentioned, the defect exists at the profile of velocity at the $X/h=0$. The WALE and Smagorinsky models are able to simulate this defect which is shown in Fig.10. Fig.11 shows the streamwise velocity on the roof at the $X/h=0.33$ that DBN model and two mentioned LES models depict a similar trend and also close agreement with the experimental data. The same comparison is shown in Fig.12 for the location of $X/h=1.66$. At these location same to $X/h=0.33$ the DBN model and LES methods have a good prediction. But for the $Y/h>1.5$ seems the prediction of WALE model is closer to experiment while for the $Y/h<1.5$ the Smagorinski model shows a better agreement with Experimental data.

The results of Smagorinski and WALE models are better than DBN model in the behind of building at the $X/h=3.66$ and $X/h=5.66$ respectively as it can be seen in Fig.13 and Fig.14. In contrary to reattachment length prediction in behind of building, the WALE model simulated the velocity in the reverse flow region with better accuracy relative to Smagorinski model.

Although the numerical results of present work for LES are in better agreement with experimental data compared with RANS models but it should be emphasized that this preference is not remarkable. The main reason for this few

improvement is the low resolution of the numerical grid. Using a finer grid was not possible because of limitation in availability of high performance computers but based on experience of the authors, performance of the LES technique can be remarkably improves with a higher resolution grid for present problem.

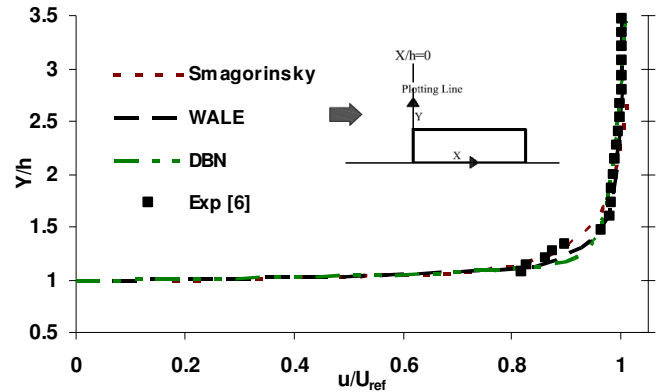


Fig.10: Streamwise velocity distribution above the building at $X/h=0$

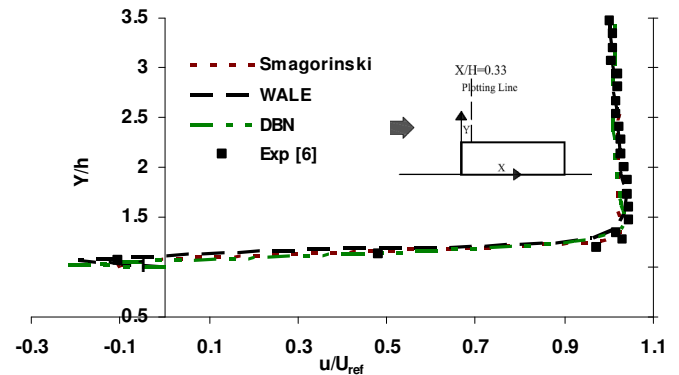


Fig.11: Streamwise velocity distribution above the building at $X/h=0.33$

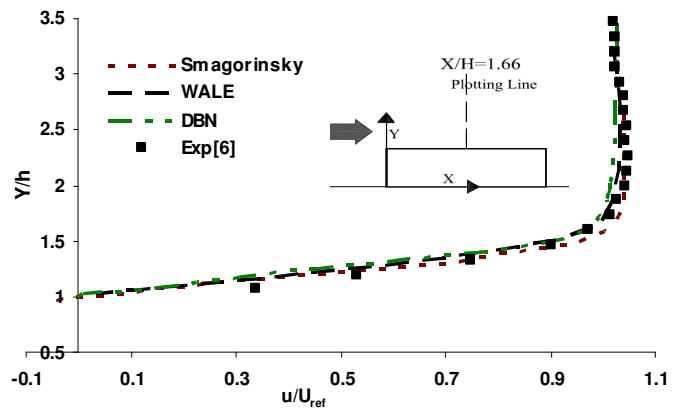


Fig.12: Streamwise velocity distribution above the building at $X/h=1.66$

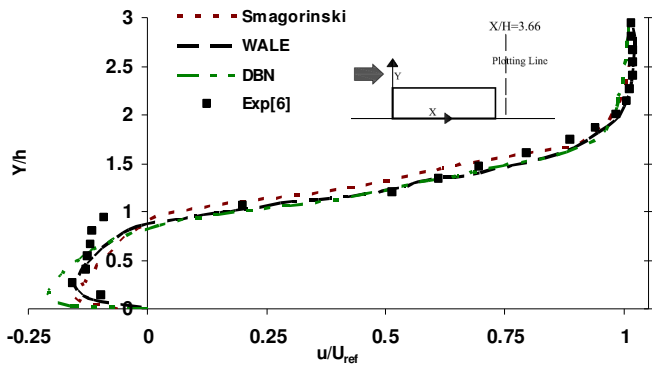


Fig.13: Streamwise velocity distribution above the building at $X/h=3.66$

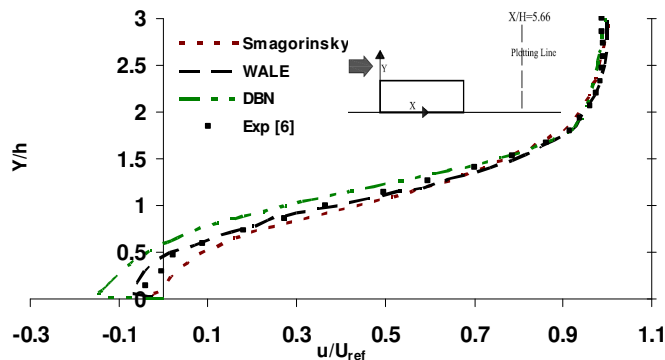


Fig.14: Streamwise velocity distribution above the building at $X/h=5.66$

CONCLUSION

1) The RANS models studied here with wall function boundary condition could not reproduce the reverse flow on the roof. This drawback was corrected by RANS models with low Reynolds boundary condition. However, except DBN model, RANS models tested here overestimated the reattachment length in behind of the building.

2) For the flowfield, the model proposed by Durbin (DBN) showed the closest agreement with the experimental data among the RANS models compared in this research.

3) The overestimation of reattachment length behind the building in DBN model was improved in Smagorinski model of LES technique. Also WALE model present a better result for streamwise velocity distribution in the recirculation zone behind the building.

4) LES technique presents a more accurate prediction compared with RANS models even for the studied coarse numerical grid. But its preference is not remarkable compared with some RANS models such as DBN model. So using a finer computational grid is strongly suggested to gain the benefits of LES technique.

REFERENCES

- [1] Rodi, W., 1997, "Comparison of LES and RANS calculations of the flow around bluff bodies," *J. Wind Eng. Ind. Aerodyn.* **69**, pp. 55-75.
- [2] Tominaga, Y., Mochida, A., Murakami, S., Sawaki, S., 2008, "Comparison of various revised k- ϵ models and LES applied to flow around a high-rise building model with 1:1:2 shape placed within the surface boundary layer," *J. Wind Eng. Ind. Aerodyn.* **96**, pp. 389-411.
- [3] Mochida, A., Tominaga, Y., Murakami, S., Yoshie, R., Ishihara, T., Ooka, R., 2002, "Comparison of various k- ϵ models and DSM applied to flow around a high-rise building—report on AIJ cooperative project for CFD prediction of wind environment," *J. Wind Struct.* **5**, pp. 227-244.
- [4] Tominaga, Y., Mochida, A., Yoshie, R., Kataoka, H., Nozu, T., Yoshikawa, T., Shirasawa, T., 2008, "AIJ guidelines for practical applications of CFD to pedestrian wind environment around buildings," *J. J. Wind Eng. Ind. Aerodyn.* **96**, pp. 1749-1761.
- [5] Iaccarino, G., Ooi, A., Durbin, P.A., Behnia, M., 2003, "Reynolds averaged simulation of unsteady separated flow, j. heat and fluid flow," **24**, pp.147-156.
- [6] Motallebi Hasankola, S.S., Goshtasbi Rad, E., Abouali, O., 2009 "Investigation the flow field around a building in wind tunnel," **12th** Fluid Dynamics Conference, Babol Noshirvani University of Technology, 28-30 April 2009.
- [7] Kato, M., Launder, B.E., 1993, "The modeling of turbulent flow around stationary and vibrating square cylinders," In: *Preprints of 9th Symposium on Turbulent Shear Flow* **10**, pp.1-6.
- [8] Murakami, S., 1993, "Comparison of various turbulence models applied to a bluff body," *J. Wind Eng. Ind. Aerodyn.* **47**, pp.21-36.
- [9] Tsuchiya, M., Murakami, S., Mochida, A., Kondo, K., Ishihara, Y., 1997, "Development of a new k- ϵ model for flow around pressure fields around bluff body," *J. Wind Eng. Ind. Aerodyn.* **68**, pp. 169-182.
- [10] Durbin, P.A., 1996. "On the k- ϵ stagnation point anomaly," *J. Heat Fluid Flow*, **17**, pp.89-90.
- [11] Wilcox, D. C. , 1998, "Turbulence Modeling for CFD," DCW Industries, Inc., La Canada, California,
- [12] Murakami, S., Mochida, A., Hayashi, Y., 1990. "Examining the k- ϵ model by means of a wind tunnel test and large eddy simulation of turbulence structure around a cube," *J. Wind Eng. Ind. Aerodyn.* **35**, pp.87-100.
- [13] Nicoud, F., Ducros, F., 1999. "Subgrid-Scale Stress Modelling Based on the Square of the Velocity Gradient Tensor". *Flow, Turbulence, and Combustion.* **62**, pp.183- 200.